Automatic surface and volume mesh generation for roughness-resolved LES of additive-manufacturing heat exchangers

Serge Meynet, Vincent Moureau, Ghislain Lartigue, Abdellah Hadjadj

AUTOMATIC SURFACE AND VOLUME MESH GENERATION FOR ROUGHNESS-RESOLVED LES OF ADDITIVE-MANUFACTURING HEAT EXCHANGERS

S. Meynet[1], *V. Moureau*[1], *G. Lartigue*[1] *and A. Hadjadj*[1]

[1] *CORIA, CNRS UMR6614, Normandie Université, UNIROUEN, INSA of Rouen, France*
serge.meynet@coria.fr

Abstract

In order to quantify the impact on the heat exchanger performances of the wall roughness introduced by additive manufacturing, roughness-resolved Large-Eddy Simulation (RRLES) is a valuable tool. However, representative rough surfaces and high-quality body-fitted grids of these surfaces are difficult to generate automatically, which prevents from building parametric RRLES databases that can be used for model development. In this work, a rough surface generator with a fine control on the height distribution in the three space directions is proposed. This tool creates triangulated surfaces that are the input of a parallel body-fitted tetrahedral mesh generator. In this latter, the cell size and its gradient and the element skewness are well controlled enabling their use for high-fidelity LES.

1 Introduction

In the aeronautical and aerospace engineering, additive manufacturing paves the way for new designs of critical components and especially heat exchangers (Carozza, 2017). Recent progresses in additive manufacturing are a great opportunity for innovation aiming at Compact Heat Exchangers (CHX). Pressure loss and heat transfer performances are the two main characteristics to be optimized for heat exchanger efficiency. However, the important roughness introduced by additive manufacturing strongly impacts these performances (Arie *et al.* 2016). There is a lack of fundamental knowledge on how these untypical roughness structures modify the heat transfer and pressure loss introducing a strong uncertainty between computer design and industrially printed parts. Reducing this uncertainty and better controlling the performance of 3D printed heat exchanger could be achieved with better rough-wall models and roughness-resolved Large-Eddy Simulation databases could help in this task. This paper focuses on how defining representative rough surfaces and how to generate 3D roughness-resolved unstructured and body-fitted meshes with a fine control on the cell size distribution.

2 Rough-surface generator (RSG)

Surface roughness parameters that characterize the height moments of a surface are categorized into three groups: amplitude, spacing and hybrid. Predominant roughness parameters commonly used in the literature are the arithmetic average height denoted S_a, the root-mean-square height S_q, skewness Sk, kurtosis Ku and the roughness density (Λ) or the effective slope ES (Gadelmawla *et al.*, 2002 ; ISO 25178-2). The arithmetic average height is the most known among the parameters and is usually used to control the roughness of manufactured parts. This is defined as the average absolute deviation of the roughness irregularities compared to the mean roughness height z_m, which is assumed to be zero throughout the paper. The root-mean-square height S_q is also another important parameter which is more difficult to measure. While skewness quantifies the asymmetry of the PDF, kurtosis describes its sharpness. Surface with high peaks or deep valleys correspond to respective positive or negative skewness. If $Ku < 3$, the distribution curve is said to be platykurtoic and has relatively few sharp peaks. In contrary if $R_{ku} > 3$, the distribution is said to be leptokurtoic and many sharp peaks are located on the surface. The case $Ku = 3$ belongs to a Gaussian PDF. Additional information is needed about the spatial properties of the surface in the other wall-tangential space directions. Studies (Napoli *et al.*, 2008 ; De Marchis *et al.*, 2015) have underlined the predominance of the effective slope in predicting roughness effects, defined as the average of the slope of the roughness along the streamwise direction:

$$ES = \frac{1}{L_x L_y} \int_{L_x} \int_{L_y} \mid \frac{\partial z(x,y)}{\partial x} \mid dxdy \quad (1)$$

Roughness in additive manufacturing

In additive manufacturing, several factors have an impact on the surface topography like the thickness of printed layers, the angle of the surface compared to the horizontal build bed, powder's particle size distribution for power bed methods or the laser power and scan speed for Selective Laser Melting (SLM), the material used and many more. For the targeted applications in this present work, surface finishing is not considered as such procedure can not be applied for CHX.

Nevertheless, one key point is that surfaces

produced with AM are likely non-Gaussian and anisotropic. Due to the layer-by-layer nature of AM process, patterns of peaks or valleys called welding tracks can be distinguished in general. Slags also appear on surface due to powder particles or material which are not correctly melted (Cabanettes *et al.*, 2018).

Numerical method

The chosen method to generate numerically rough surfaces relies mainly on the algorithm described by Hu and Tonder (1992) and with improvements from Bakolas (2003). They have developed a random surface generation approach based on Fourier analysis, filtering, and Johnson translator system (Johnson, 1947). These key points are described here.

Heightmap and areal autocorrelation function. Due to the fact that rough surfaces can be assimilated to a random process, two statistical functions are sufficient to obtain a given surface: the elevation distribution PDF and the areal autocorrelation function (AACF). The latter represents the dependence between height values at one specific location on such values at another position. It is defined as:

$$AACF(\tau_x, \tau_y) = E[z(x,y)z(x+\tau_x, y+\tau_y)] \quad (2)$$

with E the expected value of the product between height elevation at two different locations. This definition introduces two correlation lengths τ_x and τ_y respectively along the x-axis and the y-axis. They characterize the length at which the AACF drops to 10% of its nominal value in the given direction. For isotropic surfaces, these lengths are equal but their values differ for anisotropic ones.

Considering the patterns observed in additive manufacturing, only anisotropic surfaces are considered in this work. The AACF incorporated in the RSG and imposed as input is the following:

$$AACF(x,y) = S_q^2 \exp\left(-\left[\left(\frac{x}{\tau_x}\right)^2 + \left(\frac{y}{\tau_y}\right)^2\right]^{\frac{1}{2}}\right) \quad (3)$$

Filtering and Fourier analysis. The considered procedure is based on 2D digital filtering technique exposed by Hu and Tonder (1992). Such filter is a system transforming an initial $(N+n)$ x $(M+m)$ matrix $[\eta_{i,j}]$ into an output N x M matrix $[z_{i,j}]$. With *finite impulse response* (FIR) filters particularly, and given a 2D random sequence $[\eta(i,j)]$, the transformation is written as:

$$z(i,j) = \sum_{k=1}^{n}\sum_{l=1}^{m} h(k,l)\eta(i+k, j+l) \quad (4)$$

where coefficients $h(k,l)$ are to be determined for producing the expected AACF. As suggested by Hu and Tonder (1992), a windowing function $w(k,l)$ is applied onto the filter coefficients to reduce the Gibbs phenomenon. The chosen $w(k,l)$ is a Gaussian window function:

$$h_w(k,l) = h(k,l)w(k,l) \quad (5)$$

The Fourier transformation of the equation (4) yields:

$$Z(w_x, w_y) = H(w_x, w_y)A(w_x, w_y) \quad (6)$$

Fourier transform of z and η are respectively Z and A. The transfer function H can be calculated with the relation between power spectral densities (PSD) of η (S_η) and z (S_z):

$$S_z(w_x, w_y) = \mid H(w_x, w_y) \mid^2 S_\eta(w_x, w_y) \quad (7)$$

As $[\eta(i,j)]$ is considered being a Gaussian sequence, the PSD S_η is equal to a constant value. S_z corresponds to the Fourier transformation of the expected AACF. An inverse Fourier transformation applied on $H(w_x, w_y)$ gives the filter coefficients $h(k,l)$.

For anisotropic non-Gaussian surfaces, another transformation step applied to the sequence η is required to give a non-Gaussian sequence η'. This is done through a so-called Johnson translator system (Johnson, 1947). The root-mean-square S_q is conserved but new skewness $Sk_{\eta'}$ and kurtosis $Ku_{\eta'}$ factors have to be modified for η'. A convolution between filter coefficients and this new sequence yields desired S_q, Sk, Ku and AACF for the output surface $z(i,j)$.

The Johnson curves are integrated in the outer-loop algorithm given by Hill *et al.* (1976) and modified by Tuenter *et al.* (2001) to determine the parameters S_U of the Johnson curves.

Implementation of periodic boundaries

Useful for some cases, a procedure for ensuring periodic boundaries with continuous slope has to be integrated into the RSG as exposed in Fig. 1.

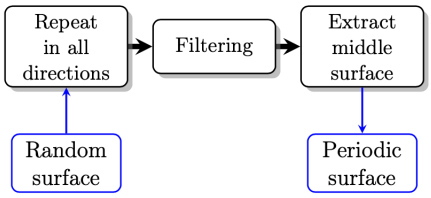

Figure 1: Procedure for obtaining periodic boundaries

First, the desired planar surface is repeated in x- and y-directions. Then a 2D Savitzky-Golay filter is applied on the global surface. This kind of filter is widely known for signal processing. Finally, we extract the half of the surface in each direction which ensures the periodicity.

Generated surfaces and geometries

The RSG has been applied successfully to periodic and non-periodic planar surfaces, parallel planes, square and cylindrical channels. Furthermore, unmelted particles and slags are present on the surface

topography in AM. Thus, a union of spheres procedure has been incorporated as an option to enable this characteristic of AM surfaces. Examples of these geometries are shown in Fig. 2.

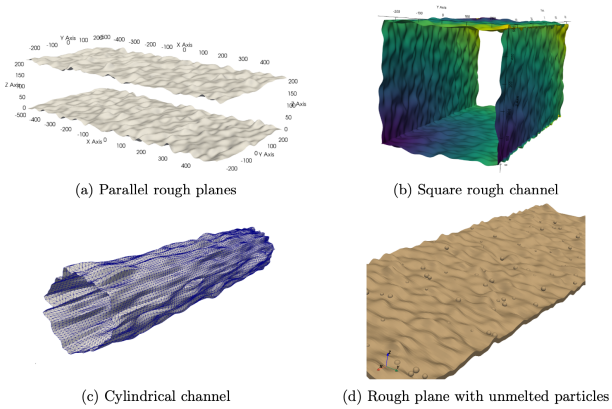

(a) Parallel rough planes (b) Square rough channel

(c) Cylindrical channel (d) Rough plane with unmelted particles

Figure 2: Examples of geometries generated with the RSG

Performances and limitations

In the surface generation process, many Gaussian series have to be generated until the transformed data set matches the required statistical parameters. Then, as a high precision is required on the generated surface properties, a lot of series are necessary. This is why we have introduced a threshold on desired values for skewness and kurtosis. This threshold corresponds to $+/-5\%$ of the target value. For the testing of the RSG, several planar surfaces were generated with different roughness parameters and correlation lengths values. The spacing along x-axis and y-axis is 2 μm and the AACF used is written in equation 3. In addition, some results on performances are presented in the table 1. The chosen correlation lengths for these tests are τ_x = 50 μm, τ_y = 20 μm.

	Parameters	Input	Output	Error(%)
Case 1	Sk	0.100	0.098	2.00
	Ku	4.00	3.80	5.00
Case 2	Sk	0.400	0.397	0.75
	Ku	4.00	3.86	3.50
Case 3	Sk	0.400	0.417	4.25
	Ku	5.00	5.05	1.00

Table 1: Performance tests on skewness and kurtosis

3 Resolved-roughness mesh generator (RRMG)

Once the STL surface is generated, meshing is a critical step for predictive roughness-resolved LES. The challenge lies in the strict control of both the mesh size and quality. The size is important as it gives the cut-off between the resolved and modeled scales. The cell-size gradient is also important as it may lead to space commutation errors in LES or to local mesh quality issues. Finally, the mesh quality, often measured through the cell skewness, has to be good enough to avoid introducing numerical errors in the finite-volume schemes. This is why a fully-automatic and well-controlled procedure for generating roughness-resolved meshes is required. The idea is that both the fluid and solid domains have to be discretized with body-fitted tetrahedral-based meshes with a controlled resolution at the wall.

Principle

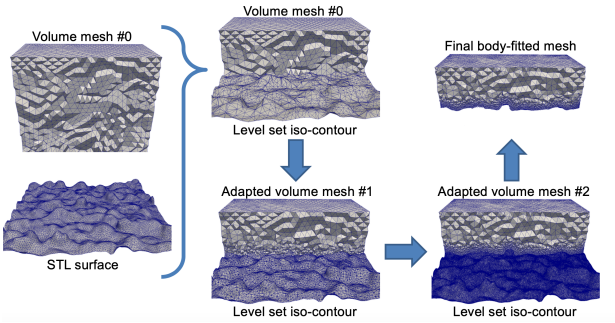

Figure 3: General principle of the RRMG

The RRMG, whose principle is exposed in Fig.3, is a volume-based mesh generator. It is not strictly a mesh generator as it requires a coarse input mesh that will be modified and cut to obtain the final mesh. The RRMG is based on many features available in the YALES2 code. YALES2 is an unstructured low-Mach number code developed at CORIA for the Direct Numerical Simulations and Large-Eddy Simulations in complex geometries (Moureau *et al.*, 2011). It heavily relies on the parallel volume and surface mesh adaptation developed jointly with INRIA, LEGI and SAFRAN TECH. This adaptation provides a fine control on the cell size and its gradient over the volume and at the roughness surface. However, the mesh adaptation requires to know where to adapt the mesh in the coarse initial mesh, i.e. where the resolved-roughness boundary is located. To this aim, many other features of YALES2 are used: handling of partitioned triangle sets similar to STLs, level set creation and displacement, computation of geometric distance to a level set or to triangles in parallel on unstructured grids, ... All these features participate to the process which is exposed hereafter. Given one or several STL files, one has to prescribe a desired cell size per STL and the name of the new boundary condition which will be created. One or several interior points have to be prescribed in order to distinguish between the interior and the exterior of the surface (fluid or solid).

Numerical procedure of the RRMG

Step 1: Reading of the STL surface and distribution on processors.

The first step of the process is the reading of the STL files and a first isotropic adaptation step in order

to get enough triangles to perform the distribution onto the processors. The isotropic STL file adaptation is performed in the code with calls to the MMGS adaptation library. Then, the STL is colored with the METIS library and distributed. Each group of triangles is represented as a master sub-surface on one processor and several slave or ghost surfaces on the other processors which also have a bounding box which crosses the one of the sub-surface. From the initial surface generated with the RSG illustrated in Fig. 4, the refinement and the distribution are represented in Fig. 5. This distribution mechanism is essential to get good performances on a large number of processors.

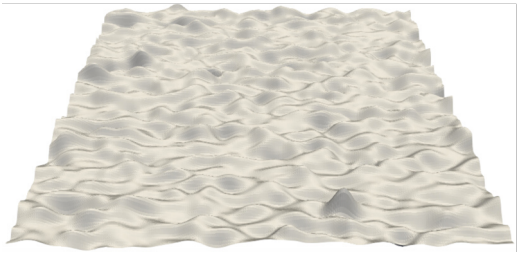

Figure 4: Original STL file

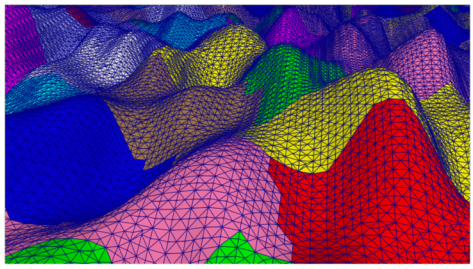

Figure 5: Refinement of the surface

Step 2: Generation of Lagrangian markers from the surface.

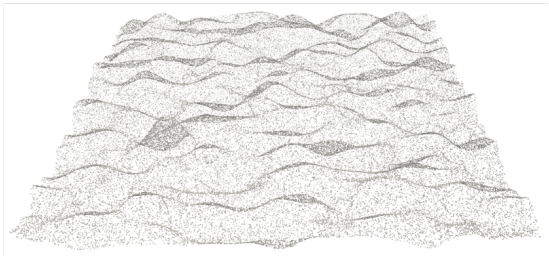

Figure 6: Lagrangian particles for the calculation of approximate and exact distance

Once the STL file is read, refined and distributed on the processors, lagrangian particles are created at the triangle barycenter and at the nodes of the master surfaces as shown in Fig. 6. These lagrangian particles carry some data as the original triangle node coordinates and the desired cell size but, they are easier to handle than triangles. These particles are relocated on the grid to find to each cell they belong and they can then be used to compute approximate distance, i.e. the minimum distance of a node of the mesh to the particles, or an exact distance based on the projection on the triangles carried by the lagrangian particles.

Step 3: Computation of approximate distance to surface.

After the particles are relocated on the volume mesh, the approximate distance of each node of the volume mesh to the surface is computed. This distance is used to build the desired cell size in the volume.

Step 4: Volume adaptation of the Eulerian mesh.

With the approximate distance, the cells in the vicinity of the surface can be refined by defining a specific metric field. This metric field is smaller at the surface location and has to respect a maximum cell size gradient condition. In order to keep a good quality of the volume mesh, several successive steps are performed. At the final step, the metric at the surface is equal to the desired cell size. The number of steps can be adjusted depending on the ratio between the cell size of the initial mesh and the final desired cell size at the surface. For the moment, the interior and the exterior of the final flow domain are not distinguishable and the cells close to the surface do not coincide with it.

Step 5: Calculation of a levelset function from interior points and markers.

In order to ultimately get a body-fitted mesh, the surface has to be materialized in the unstructured mesh. To this aim, an implicit representation of the surface is created thanks to a distance-based level set method. In this method, a signed distance function has to be generated. The surface is then the zero iso-contour of this level set. Building a distance function, which is positive on both sides of the surface is trivial. However, building a signed-distance function is more challenging. The chosen algorithm here is based on a level set displacement. The algorithm is the following:

- a geometric distance to the lagrangian particles is computed in a narrow band around the surface. This parallel algorithm is based on a fast-marching method (Janodet *et al.*, 2019). The idea is to build at each node the list of the closest lagrangian particles to the surface. The distance is then obtained by projecting the node position onto the triangles represented by the lagrangian particles.

- the desired cell size is substracted from the geometric distance creating a small negative distance region around the surface. This step creates two zero iso-contours of the level set around the surface.

- from the interior points and based on the volume

mesh connectivity, the interior domain up to the first level set is flagged and kept. The remaining domain is given a negative distance. At the end of this step, only one level set remains.

- The remaining level set is displaced back by adding the desired cell size.

While this methodology gives an approximate description of the surface on the volume mesh, the errors have been assessed and they are small and of the order of a fraction of the desired cell size. The great benefit of using a level set is that it automatically corrects some topology issues of the STL files. Since the algorithm is distance-based, no topological properties is needed for the STL files.

Step 6: Cutting of the Eulerian mesh.

Once the signed-distance level set function is built, the Eulerian mesh is cut, i.e. that all the edges, faces and cells which are crossed by the level set function are tessellated in order to transform the implicit surface into an explicitly meshed surface. In a tetrahedron, the cutting algorithm has to consider the number of edges that are crossed by the level set (3 or 4 edges). Then, to have a fully parallel algorithm, a global index of the nodes has to be considered in order to have compatible faces between two cut elements that share a parallel interface.

Step 7: Removal of the outer cells.

After the cut, the outer cells that are already flagged can be removed from the volume mesh. This step requires to rebuild some connectivity in parallel and to distribute the grid again onto the processors to keep good performances.

Step 8: Volume/surface adaptation of the interior Eulerian grid.

The mesh that undergoes the preceding steps is of good quality inside the volume but of very poor quality at the surface as the mesh cut generates very small edges and potentially highly skewed elements. Then, parallel volume and surface adaptation is performed with the MMG library to recover a correct mesh. The final mesh is represented in Fig. 7.

Assessment of final mesh

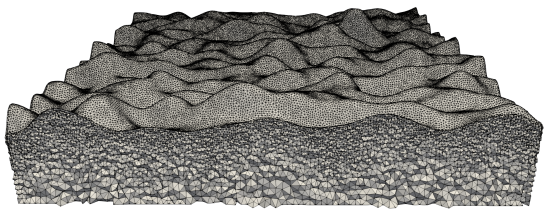

Figure 7: Final mesh after surface/volume adaptation.

The final mesh obtained at the end of the full generation process and illustrated in Fig. 7 is assessed in this section. To this aim, the skewness distribution and the cell-size distribution based on the cell volume are given in Fig. 8 and 9. To minimize the truncation errors of the finite-volume schemes of YALES2, it is necessary that a mesh contains cells which the maximum skewness is below 0.8. The obtained skewness distribution shows that the number of cells with high skewness is very limited and the distribution is centered around 0.25. The cell-size distribution is also representative of what is prescribed. A large number of cells have the prescribed cell size at the interface and the cell size grows fast to the size in the original grid.

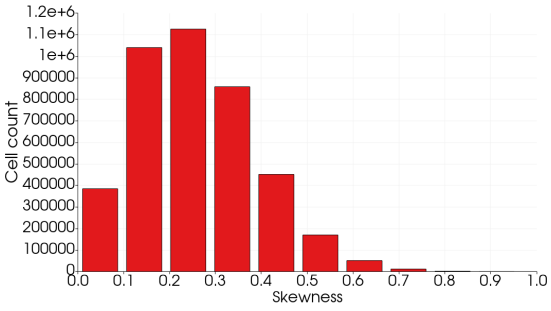

Figure 8: Skewness distribution

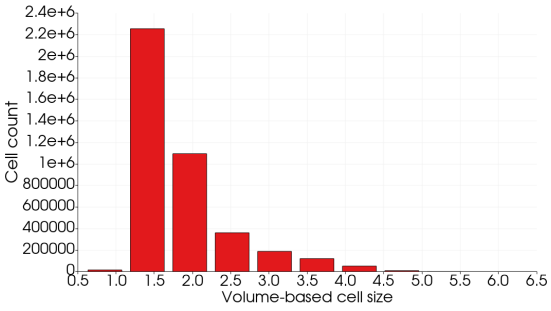

Figure 9: Cell size based on the volume $V^{1/3}$

Performances

The performances of the RRMG are assessed on two cases consisting of parallel planes with different effective slopes: $ES = 0.24$ and $ES = 0.72$. The performances are given in Table 2.

	ES	Cells	CPUs	CPU hours	RAM /CPU
Case 1	0.24	82M	560	930h	1205Mb
Case 2	0.72	67M	280	812h	1690Mb

Table 2: Meshing performances

Resolved-Roughness Large-Eddy Simulation (RRLES)

To demonstrate the properties of the surface/mesh generation process, the RRLES of the channel with two rough parallel planes and with the effective slope $ES = 0.24$ (cf table 2) is conducted.

Parameters	Values
$L_x, L_y, L_z\ (mm)$	$8.0; 3.0; 2.0$
initial N_x, N_y, N_z	$400\ ;\ 150\ ;\ 100$
Cell size on STL	$10\ \mu m$
Max cell size gradient	0.1
Number of elements	$82\ M$

Table 3: Parameters of the RRLES

The mesh properties are summarized in Table 3. The flow is assumed incompressible, the fluid kinematic viscosity is set to $\nu = 1.517\ 10^{-5}\ m^2/s$ and the maximal CFL number used is equal to 0.8. The turbulence model is the WALE sub-grid scale model (Nicoud and Ducros, 1999). A recycling boundary condition enables to make the flow periodic in the streamwise direction while slip walls are used on the side walls and no-slip walls are imposed on the rough surface. The shear Reynolds number is defined as $Re_\tau = \frac{u_\tau h}{\nu}$ with h the half channel height, and u_τ the friction velocity based on the streamwise pressure gradient. The chosen value for the present case is $Re_\tau = 970$. With these parameters, the maximum non-dimensional wall distance of the first point in the flow y^+ is less than 5.

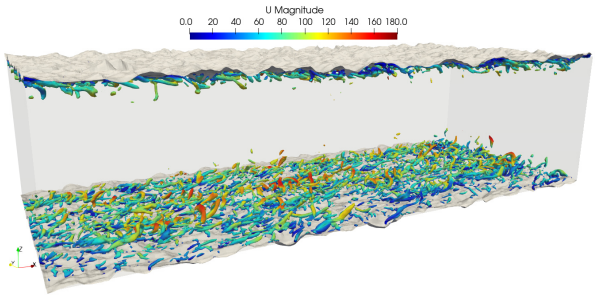

Figure 10: Q-criterion iso-contours in the RRLES

Figure 10 shows Q-criterion iso-contours to illustrate the vortical structures at the wall vicinity. This case is part of a larger database that is being built.

4 Conclusions

The surface and mesh generators have been presented in detail as well as their capabilities in this paper. They are required to create automatically body-fitted meshes of resolved roughness with imposed parameters. The rough surface generator (RSG), based on some roughness parameters, is able to accurately yield different types of roughness and different geometries in the STL format. An option for periodic boundaries with continuous slope was also introduced. Concerning the resolved-roughness mesh generator (RRMG), the procedure is fully-automatic and enable a control on the cell size at the wall. Both fluid and solid domains are discretized. Thus body-fitted tetrahedral-based meshes with a good quality are obtained with the RRMG and resolved-roughness Large-Eddy simulations can be therefore performed.

Acknowledgments

The STREAM project has received funding from the Clean Sky 2 Joint Undertaking (JU) under grant agreement No 865378. The JU receives support from the European Union's Horizon 2020 research and innovation program and the Clean Sky 2 JU members other than the Union. This abstract reflects only the authors' view, the Joint Undertaking is not responsible for any use that may be made of the information it contains.

References

Arie, M.A., Shooshtari, A.H., Dessiatoun, S.V. and Ohadi, M.M. (2016), Performance Characterization of an Additively Manufactured Titanium (Ti64) Heat Exchanger for an Air-Water Cooling Application, *Proceedings of the ASME 2016 Heat Transfer Summer Conference*

Bakolas, V. (2003), Numerical generation of arbitrarily oriented non-Gaussian three-dimensional rough surfaces, *Wear*, Vol. 254, pp. 546–554.

Carozza, A. (2017), Heat Exchangers in the Aviation Engineering, *Heat Exchangers - Advanced Features and Applications*

De Marchis, M., Milici, B. and Napoli, E. (2015), Numerical observations of turbulence structure modification in channel flow over 2D and 3D rough walls, *Int J. Heat & Fluid*, Vol. 56, pp. 108–123.

Gadelmawla, E.S., Koura, M.M., Maksoud, T.M.A., Elewa, I.M. and Soliman, H.H. (2002), Roughness parameters, *J. Materials Processing Technology*, Vol. 123, pp. 133–145

Hill, I.D., Hill, R. and Holder, R.L. (1976), Algorithm AS 99: Fitting Johnson Curves by Moments, *Applied Statistics*, Vol. 25(2), p. 180.

Hu, Y.Z. and Tonder, K. (1992), Simulation of 3-D random rough surface by 2-D digital filterand Fourier analysis, *Int. J. Mach. Tools Manulact*, Vol. 32, pp. 83–90

Janodet, R., Vaudor, G., Lartigue, G., Bénard, P., Moureau, V. and Mercier, R. (2019), An unstructured conservative level-set algorithm coupled with dynamic mesh adaptation for the computation of liquid-gas flows, *29th European Conference on Liquid Atomization and Spray Systems*

Johnson, N.L. (1949), Systems of Frequency Curves Generated by Methods of Translation, *Biometrika*, Vol. 36(1/2), p. 149.

Moureau, V., Domingo, P. and Vervisch, L. (2011), Design of a massively parallel CFD code for complex geometries, *Comptes Rendus Mécanique*, Vol. 339(2-3), pp. 141–148.

Napoli, E., Armenio, V. and De Marchis, M. (2008), The effect of the slope of irregularly distributed roughness elements on turbulent wall-bounded flow, *J. Fluid Mech*, Vol. 613, pp. 385–394.

Nicoud, N. and Ducros, F. (1999), Subgrid-scale stress modelling based on the square of the velocity gradient tensor, *Flow, Turbulence and Combustion*, Vol. 62 (3), pp. 183-200.

Tuenter, H.J.H. (2001), An algorithm to determine the parameters of SU-curves in the johnson system of probabillity distributions by moment matching, *J. Statistical Computation and Simulation*, Vol. 70(4), pp. 325–347.